Supporting information for: Bulk Heterojunction Morphologies with Atomistic Resolution from Coarse-Grain Solvent Evaporation Simulations

Riccardo Alessandri,[†,‡] Jaakko J. Uusitalo,[†,‡] Alex H. de Vries,[†,‡] Remco W. A. Havenith,[†,¶,§] and Siewert J. Marrink[*,†,‡]

†*Zernike Institute for Advanced Materials, University of Groningen, Nijenborgh 4, 9747 AG Groningen, The Netherlands*

‡*Groningen Biomolecular Sciences and Biotechnology Institute, University of Groningen, Nijenborgh 7, 9747 AG Groningen, The Netherlands*

¶*Stratingh Institute for Chemistry, University of Groningen, Nijenborgh 4, 9747 AG Groningen, The Netherlands*

§*Ghent Quantum Chemistry Group, Department of Inorganic and Physical Chemistry, Ghent University, Krijgslaan 281 (S3), B-9000 Gent, Belgium*

E-mail: s.j.marrink@rug.nl

Comparison to EFSEM Image

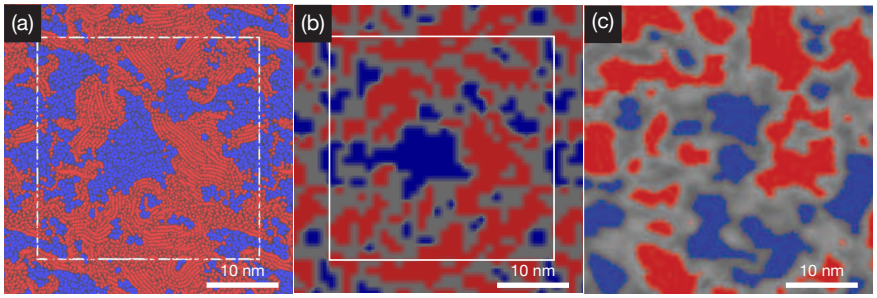

Figure S1: Comparison between the (a) single-layer CG morphology, (b) the corresponding 2.5 nm thick spatially discretized image and (c) a close up of an EFSEM image of a spin-coated blend taken by Masters et al.[S1] (close up of Figure 7c of Ref. S1 reproduced under the Creative Commons Attribution 4.0 International License).

Rendering of Morphologies During Annealing

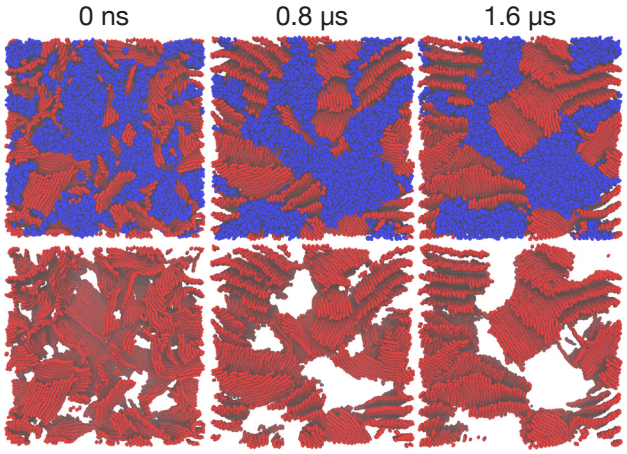

Figure S2: Snaphots at different times of the annealing process with (top) and without (bottom) the PCMB phase. Only P3HT backbones are shown to highlight the increased ordering in the P3HT phase upon annealing.

Annealing as a Function of P3HT MW

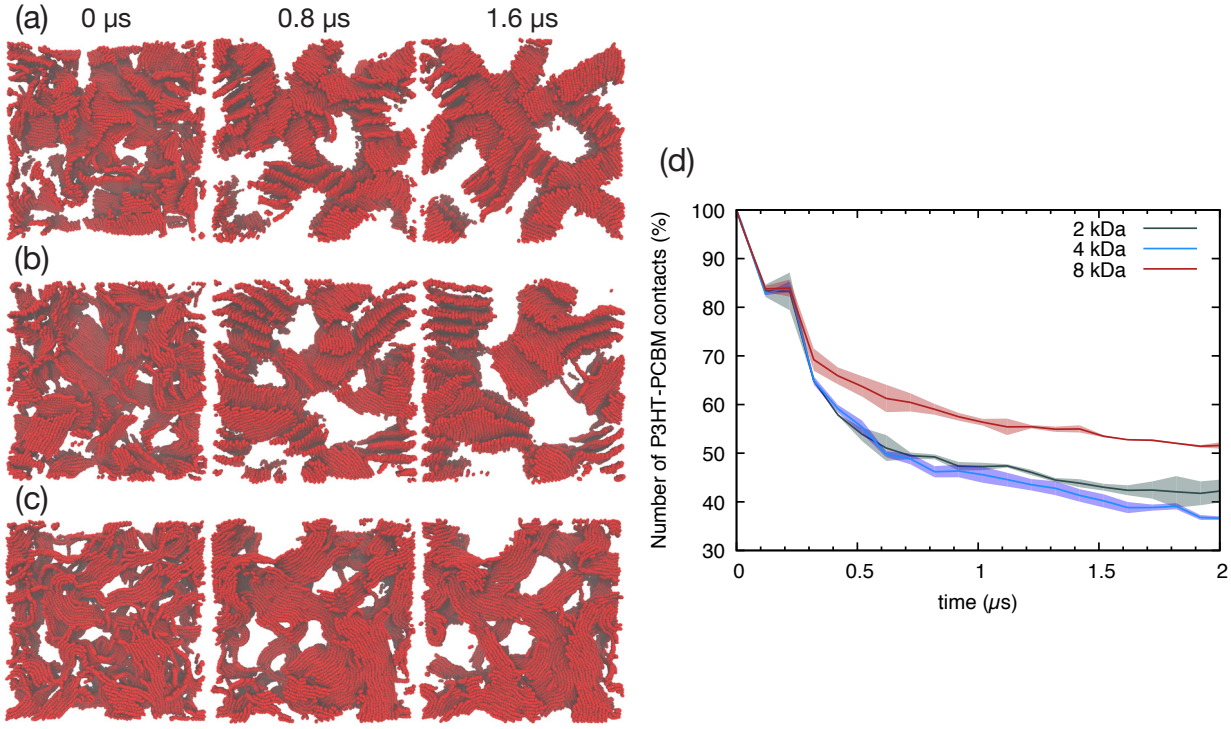

Figure S3: On the left-hand side, snaphots at different times during the annealing process are shown for P3HT:PCBM blends with varying P3HT MW: (a) 2 kDa, (b) 4 kDa and (c) 8 kDa. Only P3HT backbones are shown. White areas denote the location of P3HT side chains or PCBM domains. The % of P3HT-PCBM contacts as a function of the annealing time (right) is also shown for the three cases. The % of number of P3HT-PCBM contacts is normalized to the initial dried morphologies, so that the amount of P3HT-PCBM contacts before the annealing are taken as the 100%. The % of contacts then decreases as the blends are annealed because of phase segregation.

Force Fields Details

Coarse-Grain Models

P3HT. The oligothiophene amphiphile Martini model[S2] has been used as starting point for the P3HT CG model. A few important changes have been made to the mapping of thiophene so to realize a model which is transferable, in the spirit of the Martini CG force field. The mapping of thiophene is critical as it represents a case in which the exception to the 4-to-1 Martini mapping rule admitted for the necessity to mantain the symmetry of the ring structure come down to a mapping of the 5 thiophene heavy atoms to 3 CG sites. This mapping implies bond distances of about 0.2 nm when the bonds are extracted from atomistic trajectories. However, beads being so close to each other give rise to a region with a *high energy density*: another CG molecule coming into the interaction radius with such region will be overly attracted by it, resulting on a disbalance of the carefully parametrized Martini partioning equilibria. For this, bond distances have been increased by 20% (up to 0.24 nm). This also improves the shape of thiophene CG model, otherwise approaching too much an ellipsoidal shape.

The bead types, which define the nonbonded interactions, have been chosen on the basis of free energy of transfer data. Based on the new thiophene CG bond distances, three SC5 have been found to reproduce experimental transfer free energies for the five-membered ring (see Table S6); the hexyl side chain is described by two SC3 beads. A representation of the Martini mapping and underlying atomistic structure is presented in Figure S4, and bond and angle distributions are presented in Figure S5. The CG force field bonded parameters are collected in Table S1. Very stiff bonds, such as the ones between groups which are part of ring structures, are modeled as constraints. Virtual sites (VSs) are defined at the center of mass of the thiophene rings in order to have more control on the polymer backbone. For example, angles between VSs and neighbouring thiophene SC5 beads are introduced in order to preserve planarity. A VS-assisted dihedral ensures the distribution of dihedral angles

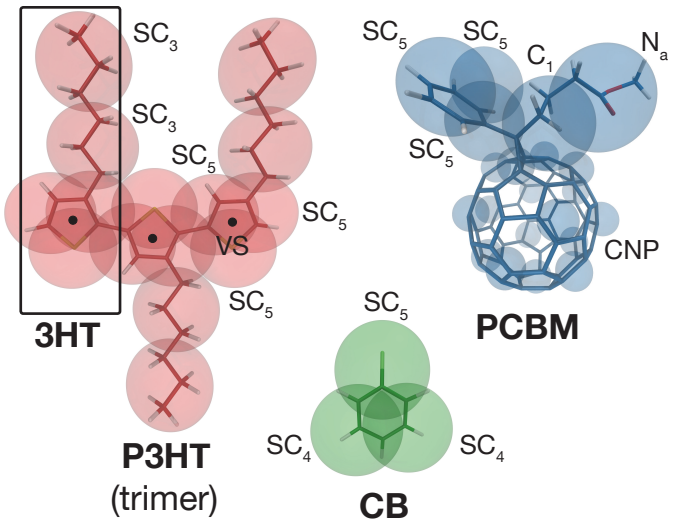

Figure S4: CG site positions (and types) and underlying atomistic structures for the molecules involved in the present study. The Martini model beads describing C_{60} are depicted with a smaller radius for clarity.

Table S1: P3HT CG bonded parameters. The indices i, j and k indicate that the bonded term is defined between subsequent thiophene units.

	Bead types (labels)	b_0 (nm)	κ_b (kJ mol^{-1} nm^{-2})	
b_1	SC5-SC5 (S1-C2, S1-C3, C2-C3)	0.240	constraint	
b_2	SC5-SC3 (C3-C5)	0.285	constraint	
b_3	SC3-SC3 (C5-C6)	0.360	5000	
b_4	VS_i-VS_j (VS_i-VS_j)	0.380	50000	
		θ_0 (deg)	κ_θ (kJ mol^{-1})	
θ_1	SC5-SC5-SC3 (S1-C3-C5)	180	250	
θ_2	SC5-SC3-SC3 (C3-C5-C6)	155	25	
θ_3	VS_i-$SC5_j$-$SC5_j$ ($V4_i$-$C3_j$-$C5_j$)	160	180	
θ_4	VS_i-VS_j-VS_k ($V4_i$-$V4_j$-$V4_k$)	158	180	
		ϕ_0 (deg)	κ_ϕ (kJ mol^{-1})	n
ϕ_1	$SC5_i$-VS_i-VS_j-$SC5_j$ ($S1_i$-$V4_i$-$S1_j$-$V4_j$)	0.00	1.80	1
		0.00	-9.50	2

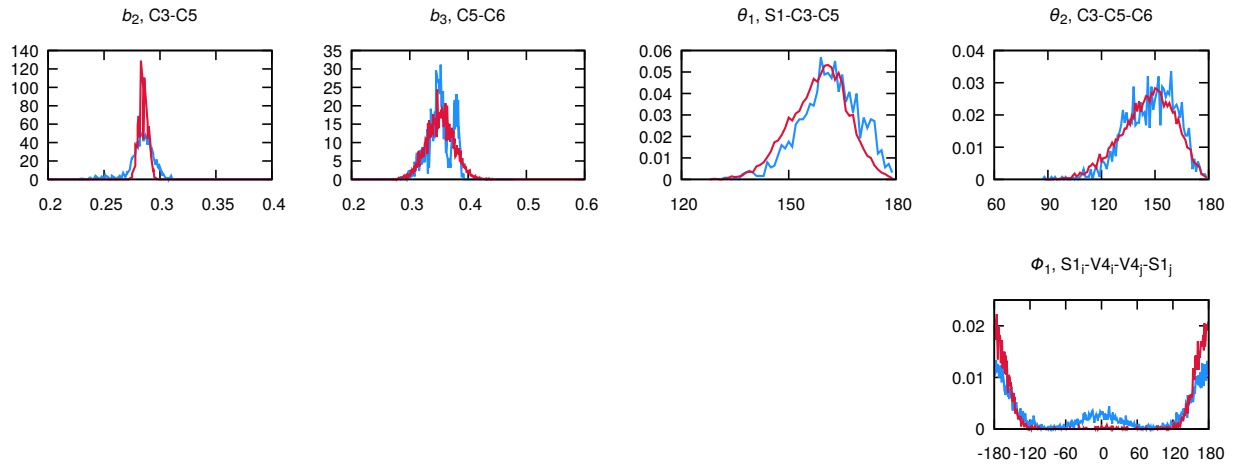

Figure S5: Bond and angle distributions for P3HT (Martini in red, GROMOS in blue). Each header indicates the degree of freedom whose distribution is shown (compare to Table S1).

between thiophene rings match the atomistic one; the latter having been fit to quantum mechanical (QM) calculations (see Section **Atomistic models**). This strategy also improves numerical stability.[S3] Note that P3HT molecular weight polydisperisity can be introduced by simply adding a mixture of chains with different molecular weights (*i.e.*, the current CG force field can be used as it is). Introducing polydispersity in the regio-regularity requires, however, some modification of the force field. Namely, the current inter-thiophene dihedral potentials, optimized based on QM calculations for the head-tail case (that is, the regio-regular case), may not be appropriate. An investigation of the change on the dihedral potential in the head-head or tail-tail case would be necessary in order to verify whether the parameters are accurate also for simulation region-random P3HT. The density of the Martini 3HT model is 0.950 g cm^{-3} (computed on a box of ∼450 molecules), in good agreement with the experimental density (0.936 g cm^{-3}).

Table S2: Mass densities for the studied compounds. Outcomes of CG and AA simulations are reported along with the experimental values. All values in g cm^{-3}.

	exp.	CG	AA
3HT	0.94	0.95	1.02
PCBM	∼1.50	1.37	1.55
CB	1.10	0.90	1.08

PCBM. The CG model of PCBM makes use of the Martini "F_{16}" model, a 16 beads representation of C_{60} fullerene developed by Monticelli[S4] and available on the web.[S5] The phenyl-butyric acid methyl ester side chain is represented by a total of five interaction sites: three Martini SC5 particles represent the phenyl moiety, following the standard model for benzene, while the butyric acid methyl ester side chain is modelled with a C1 (butane) and Na (ester) particles (see also Figure S4). The bonded parameters for the PCBM CG model are collected in Table S3, while bond and angle distributions are presented in Figure S6. The

Table S3: PCBM CG bonded parameters.

	Bead types (labels)	b_0 (nm)	κ_b (kJ mol^{-1} nm^{-2})	
b_1	CNP-SC5 (C08-C17)	0.290	constraint	
b_2	CNP-C1 (C08-C20)	0.295	50000	
b_3	SC5-C1 (C17-C20)	0.305	20000	
b_4	C1-Na (C20-N21)	0.390	2500	
b_5	SC5-SC5 (C17-C18, C17-C19, C18-C19)	0.270	constraint	
		θ_0 (deg)	κ_θ (kJ mol^{-1})	
θ_1	CNP-C1-Na (C08-C20-N21)	150	50	
θ_2	SC5-C1-Na (C17-C20-N21)	140	25	
		ϕ_0 (deg)	κ_ϕ (kJ mol^{-1} rad^{-2})	n
ϕ_1	CNP-C1-SC5-SC5 (C08-C20-C18-C19)	−10.00	100.00	2
ϕ_2	CNP-C1-SC5-SC5 (C08-C20-C19-C18)	−50.00	100.00	2
ϕ_3	CNP-SC5-C1-CNP (C03-C17-C20-C09)	5.00	200.00	

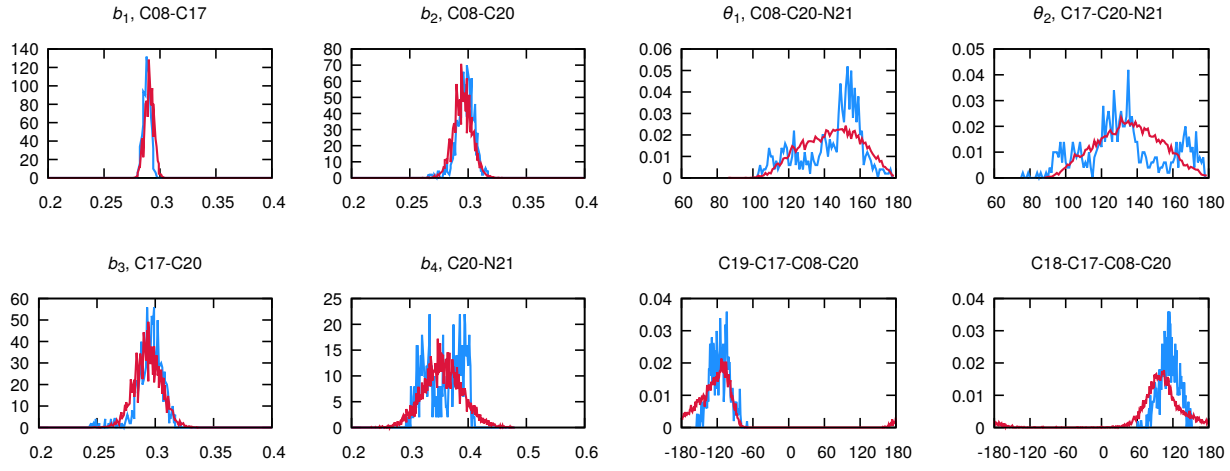

Figure S6: Bond and angle distributions for PCBM (Martini in red, GROMOS in blue). Each header indicates the degree of freedom whose distribution is shown (compare to Table S3).

dihedral angle distribution corresponding to the rotation around the bond connecting the phenyl ring to C_{60} is reproduced at the CG level due to the presence of two (proper) dihedrals ϕ_1 and ϕ_2. Note that the dihedrals plotted in Figure S6 (right-hand side, bottom) are not the same as ϕ_1 and ϕ_2, but are the ones which is better to look at when comparing to the atomistic dihedral. The (improper) dihedral ϕ_3 is added to keep the side chain orientation fixed with respect to the beads describing C_{60}. The density of the Martini PCBM model is 1.37 g cm^{-3} (for a box of $\sim$1000 molecules), about 8% too low with respect to the experimental density for an amorphous PCBM film ($\sim$1.5 g cm^{-3},[S6–S8] although there are studies[S9] reporting a lower density of about $\sim$1.3 g cm^{-3}). The density obtained for the PCBM atomistic model (see also next Section) is $\sim$1.55 g cm^{-3}, supporting the majority of experimental data. The CG model underestimation is probably mainly caused by the (too large) size of the S-beads describing the phenyl ring. This hypothesis is supported by the fact that the density of a pure benzene phase is 0.710 g cm^{-3} in the Martini model, while the experimental value 0.876 g cm^{-3}.

Chlorobenzene (CB), being the most popular solvent for the P3HT:PCBM blend along with 1,2-dichlorobenzene,[S10] has been chosen as solvent. A Martini model has been created based on the Martini benzene model. Two SC4 and a SC5 beads describe the ring (see also Figure S4), giving free energies of transfer in agreement with experimental data (see Table S6). The bonds SC4-SC4 and SC4-SC5 are modeled as constraints with lengths of 0.27 and 0.33 nm, respectively. The density obtained for such a model is 0.90 g cm^{-3}, which underestimates the actual density of CB (1.10 g cm^{-3}). However, as noted before, the same is true for the density of benzene within the Martini force field.

Atomistic Models

All-atom (AA) models based on the GROMOS 53A6 force field[S11] have been used as reference to derive effective bonded interactions for the CG ones and as reference for free energy profiles of dimerization. AA models were obtained as follows: a starting AA topology was

obtained from the automated topology builder (ATB);[S12] the obtained parameters were then thoroughly double-checked for consistency with the GROMOS 53A6 force field as defined in Ref. S11; QM calculations have been used to check critical dihedral angles; HF/6-31G* dipole preserving analysis (DPA)[S13] charges are used. Charges have been computed on a B3LYP/6-31G* optimized structure and they have been symmetrized and rounded to three decimal digits. Both geometry optimization and dipole analysis calculations have been performed with the GAMESS-UK package.[S14] More specific details on the AA models are given in the following sections for the various molecules employed in the study.

P3HT. The polymer AA model bonded parameters are shown in Table S4. When no standard GROMOS bonded parameters were available, this being the case for a few bonded terms involving the thiophene ring, the quantum-mechanically optimized structure was taken as reference for selecting a equilibrium bond (angle) distance. Force constants for such bonded terms were taken from the pool of already existing GROMOS parameters. The dihedral angle between different thiophene units (S-C-C-S) has been parametrized[S2] based on torsional energy profiles computed by Darling and Sternberg.[S15] An equilibrated simulation box containing 216 3HT monomers shows a density of 1.02 g cm^{-3}, overestimating (by about 9%) the experimental value (0.936 g cm^{-3}).

PCBM. The AA C_{60} model employed is the one developed by Monticelli,[S4] available on the web at Ref. S5. The model uses the Lennard-Jones parameters obtained by Girifalco, which were derived based on solid-state properties (heat of sublimation, lattice constant of C_{60} crystal),[S16] but which turn out to perform also reasonably well in terms of partitioning between solvents.[S4] The model for the sidechain has been obtained following the general procedure outlined before and was subsequently merged to the C_{60} model. Bonded terms for PCBM are listed in Table S5. The dihedral involving the rotation around the bond connecting the phenyl ring to C_{60} and the one involving the rotation around the bond connecting the butyric acid methyl ester moiety to C_{60} have been taken from the OPLS-AA force field[S17] following Cheung and Troisi.[S18] The density of a box (containing about 800

Table S4: P3HT atomistic bonded parameters. The indices i, j and k indicate that the bonded term is defined between subsequent thiophene units. If the bonded parameters are standard GROMOS 53A6, the corresponding GROMOS labelling is shown in parenthesis next to the bond (angle) equilibrium value and/or force constant.

Atoms	b_0 (nm)	κ_b (kJ mol^{-1} nm^{-4})	
S-C	0.1730	$5.94 \cdot 10^6$ (gb_31)	
HC-C	0.1090 (gb_3)	$1.23 \cdot 10^7$ (gb_3)	
C-C (CT2-CT3)	0.1360 (gb_13)	$1.02 \cdot 10^7$ (gb_13)	
C-C (CT3-CT4)	0.1430 (gb_19)	$9.21 \cdot 10^6$ (gb_19)	
C-C (CT3-C6)	0.1520 (gb_26)	$5.43 \cdot 10^6$ (gb_26)	
C-C (hexyl chain)	0.1530 (gb_27)	$7.15 \cdot 10^6$ (gb_27)	
C_i-C_j ($CT2_i$-$CT5_j$)	0.1430 (gb_19)	$9.21 \cdot 10^6$ (gb_19)	
	θ_0 (deg)	κ_θ (kJ mol^{-1})	
C-S-C	92.80	420.00 (ga_2)	
S-C-HC	119.00	575.00 (ga_36)	
S-C-C	110.00	530.00 (ga_15)	
HC-C-C (thiophene)	126.00 (ga_36)	575.00 (ga_36)	
C-C-C	111.00 (ga_15)	530.00 (ga_15)	
C-C-C (CT-CT-C)	126.00 (ga_37)	640.00 (ga_37)	
HC-C-C,HC (hexyl chain)	109.50 (ga_11)	425.00 (ga_11)	
C_i-C_i-C_j (thiophene)	130.00	760.00 (ga_39)	
S_i-C_i-C_j (thiophene)	120.00 (ga_29)	760.00 (ga_29)	
	ϕ_0 (deg)	κ_ϕ (kJ mol^{-1})	n
thiophene	0.00 (gi_1)	167.36 (gi_1)	
C-C-C-C (CT-CT-C-C)	0.00 (gd_40)	1.00 (gd_40)	6
C-C-C-C (hexyl chain)	0.00 (gd_34)	5.92 (gd_34)	3
S_i-C_i-C_j-S_j [a]	0.00	1.80	1
	0.00	−9.50	2

[a] fitted to QM data.

molecules) of (amorphous) PCBM is found to be 1.55 g cm^{-3}, in agreement with the majority

Table S5: PCBM atomistic bonded parameters. If the bonded parameters are standard GROMOS 53A6, the corresponding GROMOS labelling is shown in parenthesis next to the bond (angle) equilibrium value and/or force constant.

Atoms	b_0 (nm)	κ_b (kJ mol^{-1} nm^{-4})	
CF-CF (fullerene)	0.1450	$3.92 \cdot 10^5$	
CF-C	0.1529	$2.24 \cdot 10^5$	
HC-C	0.1090 (gb_3)	$1.23 \cdot 10^7$ (gb_3)	
C-C (alkyl chain)	0.1530 (gb_27)	$7.15 \cdot 10^6$ (gb_27)	
C-O (ether)	0.1360 (gb_13)	$1.02 \cdot 10^7$ (gb_13)	
C-O (carbonyl)	0.1230 (gb_13)	$1.66 \cdot 10^7$ (gb_13)	
C-C (phenyl)	0.1390 (gb_15)	$8.66 \cdot 10^6$ (gb_15)	
	θ_0 (deg)	κ_θ (kJ mol^{-1})	
CF-CF-CF (fullerene pentagons)	108.0	527.184	
CF-CF-CF (fullerene hexagons)	120.0	527.184	
CF-CF-C (fullerene - side chain)	62.8; 54.5; 120.0	488.273; 585.76; 527.184	
C-C-C	111.00 (ga_15)	530.00 (ga_15)	
HC-C-C,HC (hexyl chain)	109.50 (ga_11)	425.00 (ga_11)	
C-C-C (phenyl)	120.00 (ga_26)	530.00 (ga_26)	
C-C-CH (phenyl)	120.00 (ga_25)	530.00 (ga_25)	
C-C-O	126.00 (ga_38)	770.00 (ga_38)	
O-C-O	124.00 (ga_33)	730.00 (ga_33)	
C-O-C	120.00	635.00 (ga_22)	
	ϕ_0 (deg)	κ_ϕ (kJ mol^{-1})	n
CF-CF-CF-CF	143.00	100.00	
C-C-C-C (phenyl)	0.00 (gi_1)	167.36 (gi_1)	
C-C-C-C,HC (alkyl)	0.00 (gd_29)	3.77 (gd_29)	3
C-C-C-O, C-C-O-C (alkyl)	180.00 (gd_11)	7.11 (gd_29)	3
	Fourier dihedral coefficients (kJ mol^{-1})		
CF-C-C-C (fullerene-alkyl)	0.000 0.000	0.000 0.000	
CF-C-C-C (fullerene-phenyl)	5.439 −0.209	0.837 0.000	

of the experimental reports.[S6–S8]

The CB AA model gives a density of 1.08 g cm^{-3}, which agrees well with the experimental value of 1.11 g cm^{-3}.[S19] GROMACS topology files of the Martini and atomistic models used in the present work are available for download as part of the Supporting Information and on the Martini portal http://cgmartini.nl.

Force Field Validation

Free Energy of Transfer. Partitioning between different solvents being the main target of the Martini force field parametrization, transfer free energies of the newly created molecules have been computed and compared to experimental or atomistic data in order to choose the nonbonded interactions. Along with the commonly employed partitioning between hexadecane and water, partitioning data between hexadecane and benzene have been included (for the fragments for which experimental data were available) because of the relevance of benzene as a phase for the pi-conjugated systems under study. Computed free energies of transfer have been obtained by separately calculating the solvation free energies in the various solvents and then using the following thermodynamic cycle

$$\Delta G_{\mathrm{S}_1 \to \mathrm{S}_2} = \Delta G_{\mathrm{S}_1 \to \emptyset} - \Delta G_{\mathrm{S}_2 \to \emptyset}$$

where S_i denotes a solvent and Ø denotes vacuum, to compute the free energy change in moving the solute from S_1 to S_2. Solvation free energies were computed by gradually decoupling the solute from the solvent, that is, by simulating the desolvation of the solute. The change in free energy between the solvated and the fully uncoupled state is the negative of the solvation free energy. The degree of coupling between solvent and solute is changed through the use of the λ parameter, ranging from 1 for the solvated solute to 0 for the uncoupled state (solute in vacuum). 10 and 20 λ points were simulated for CG and AA systems, respectively. Electrostatic interactions were switched off before van der Waals ones when charged molecules were present. A stochastic integrator was used, and the velocity-rescaling thermostat[S20] and the Parrinello-Rahman barostat[S21] employed to maintain pressure and temperature, respectively. GROMACS 5.x was employed to run the simulations. The free energies and corresponding errors were finally computed using the Multistate Bennett Acceptance Ratio (MBAR).[S22] Table S6 lists the results for molecules (or moieties) involved, along with the final CG representations.

Table S6: Partitioning data for several molecules and moieties employed in this study. The free energy relative to the transfer of the solute molecule from solvent S_1 to S_2 ($\Delta G_{S_1 \to S_2}$) obtained from experiments (along with the experimentally determined partitioning coefficient logP representing the same transfer ($\log P_{S_1 \to S_2}$)) and computed at the CG and AA levels are shown. Solvents are hexadecane (HD), benzene (BZ) and water (W). All the free energies are in kJ mol^{-1}. Statistical uncertainty for the computed ΔG is below 0.3 kJ mol^{-1} in all cases; however, the accuracy of the force field being considered to be at most 1 kJ mol $^{-1}$, the numbers are rounded to integers. Experimental data are from Refs. S23 and S24.

		$\Delta G_{HD \to W}$				$\Delta G_{HD \to BZ}$			
	CG model	($\log P_{HD \to W}$)	exp	CG	AA	($\log P_{HD \to BZ}$)	exp	CG	AA
thiophene	SC5-SC5-SC5	(−1.78)	10	12	13				
hexane	SC3-SC3	(−4.49)	26	25	25				
benzene	SC5-SC5-SC5	(−2.15)	12	11	13	(0.47[a])	−3	0	−3
CB	SC4-SC4-SC5	(−2.84)	16	18	18	(0.33[a])	−2	1	−3
C_{60}[b]	F_{16}		97	75	92		−9	−10	

[a] Calculated (ADF COSMO-RS) value.[S24]

[b] All data from Ref. S4. Octane is used as hydrophobic phase instead of hexadecane.

PMF Calculations. The PMF profiles were obtained from umbrella sampling (US) simulations. The two molecules were placed in a box and solvated in CB. Umbrella windows were spaced 0.05 nm apart along the reaction coordinate, this being the distance between the centres of mass of the thiophene (in the case of 3HT) or of the C_{60} moiety (in the case of PCBM). Note that the box was large enough so that even at the largest distance each molecule was further away from periodic images than from the actual other molecule present in the box. For each window, this distance was kept fixed by an umbrella potential with a force constant of 1500 kJ mol^{-1} nm^{-2}. Each window was simulated for 500 ns in the case of the CG systems and 100 ns in the AA cases. A stochastic integrator was employed, and weak coupling schemes used to maintain pressure and temperature.[S25] GROMACS 4.6.7 was employed to run the US simulations and the free energy profiles were calculated using the weighted histogram analysis method (WHAM)[S26] as implemented in the GROMACS tool g_wham.

Umbrella Sampling Results. In Figure S7 all the computed PMFs are shown. Overall, the agreement between atomistic and CG models is more than satisfactory. Main discrepancies are seen for the 3HT model. By comparing the Martini 3HT monomers dimerization

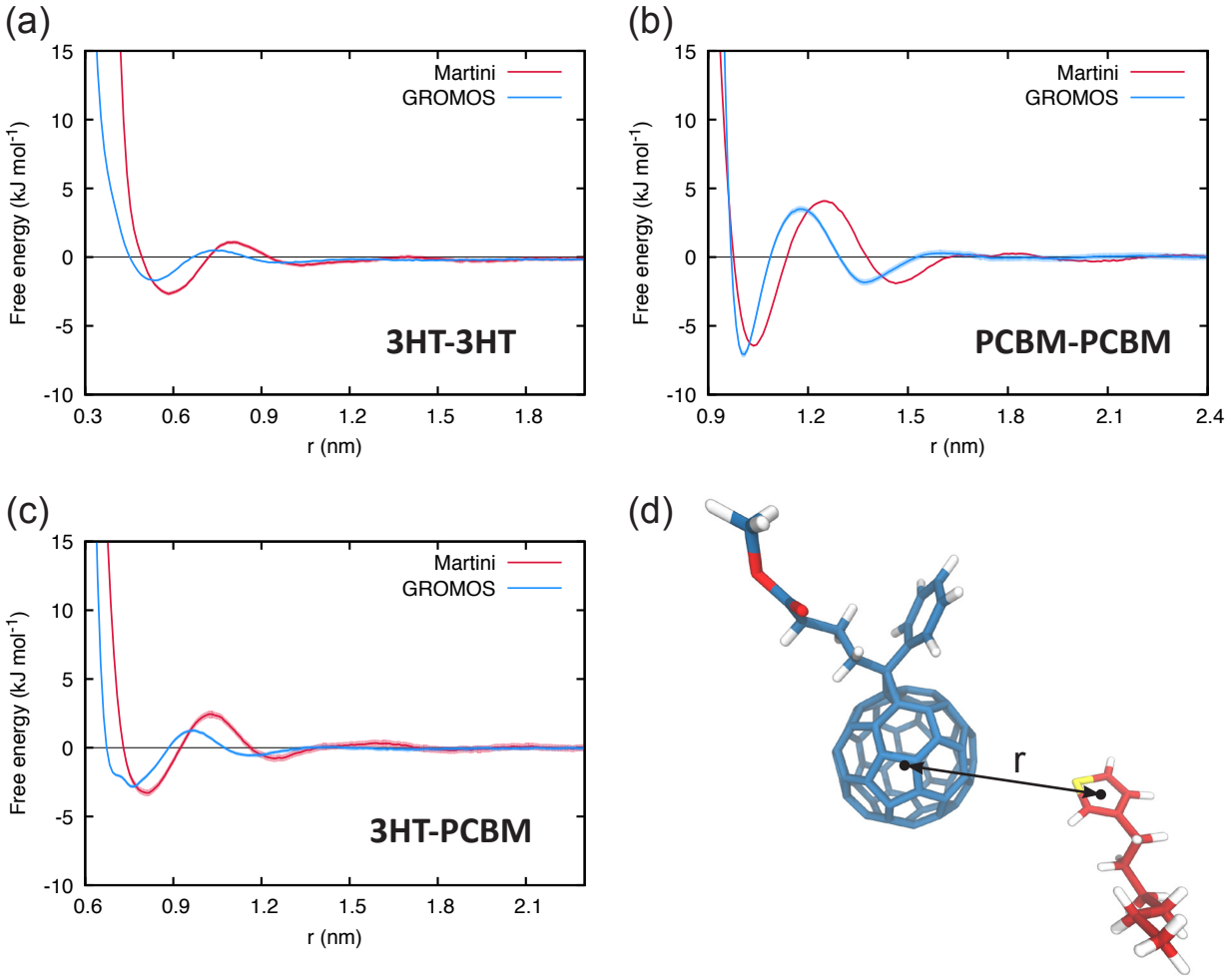

Figure S7: PMFs of dimerization for the (a) donor-donor, (b) acceptor-acceptor and (c) donor-acceptor pairs in CB. GROMOS PMFs are in blue, while Martini in red. (d) Snapshot from the 3HT-PCBM atomistic simulation showing the distance r between the centers of mass of C_{60} and the thiophene ring.

PMF to its atomistic analogue, two main features are apparent: first, the minimum is shifted towards a larger distance (∼0.59 nm versus ∼0.54 nm); secondly, the minimum is detectably deeper (about 1 kJ mol^{-1}) in the case of the CG representation of the monomeric unit. This was not unexpected. The thiophene ring is, as described before, mapped using three S-particles. These beads have a smaller radius (0.241 nm, $= \sqrt[6]{2}\sigma_S$ where $\sigma_S = 0.43$ nm)

than normal Martini beads (0.264 nm, $= \sqrt[6]{2}\sigma_N$ where $\sigma_N = 0.47$ nm) in order to account for a reduced CG sites/atoms mapping ratio. However, the size of the S-beads is still too large as compared to the "thickness" of ring systems, making so that two thiophene units cannot get as close as they can when described atomistically. Regarding the deeper minimum, thiophene, as noted previously, constitutes an extreme case where 5 atoms are mapped to 3 interaction sites, making the CG sites/atoms ratio < 2. The higher density of interaction sites (as compared to Martini standards) caused by this gives rise to somewhat stronger interactions between thiophene rings and other molecules. The interaction between two thiophene rings will be affected twice by this effect, thus causing the overestimation seen in the 3HT-3HT free energy profile. The overestimation is, however, slightly less than 1 kJ mol^{-1}, and for this considered to be in good agreement with the AA reference PMF.

Simulations Details

Evaporation Protocol Details. P3HT, followed by PCBM, molecules are randomly inserted in the simulation box and subsequently solvated in CB. Four cycles of energy minimization followed by one NVT and one NPT simulations are run. The mdp run parameters for these initial phases are the same as the run parameters described in the Methods section for solvent evaporation simulations, with the following differences. In the case of the energy minimization, 20000 steps of steepest descent are performed. For the NVT and NPT equilibrations, weak coupling schemes are employed to maintain pressure and temperature.[S25] The evaporation script and all the files necessary for the run are available for download as part of the Supporting Information and on the Martini portal http://cgmartini.nl.

Simulation Box Size. In Figure S8 top views on final morphologies obtained from evaporation simulations on different length scales are displayed. The P3HT:PCBM weight ratio is 0.7:1.0. The number of contacts have been computed for the different system size final blends and are collected in Table S7. It can be seen as the percentages of the computed contacts remain practically constant as the system size increases.

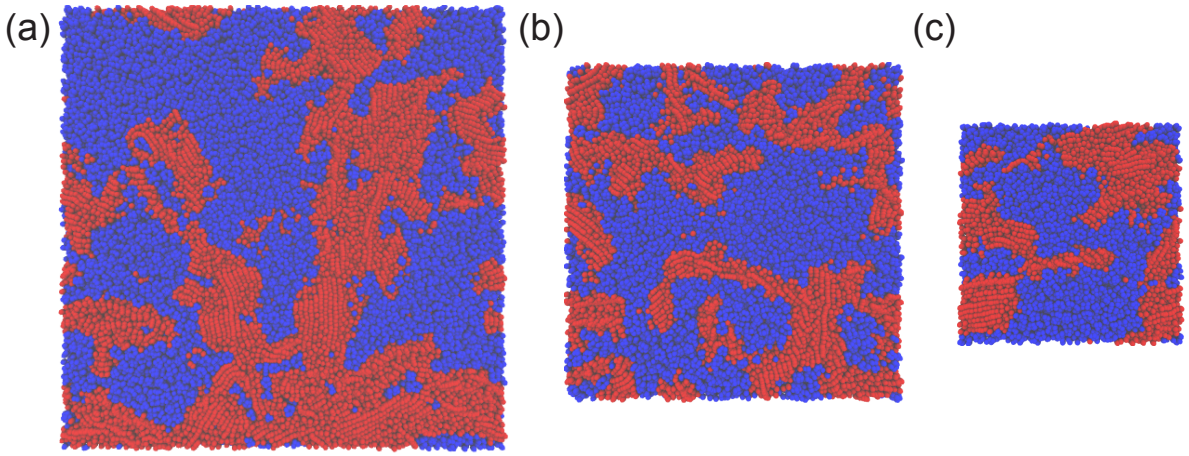

Figure S8: Top view of morphologies for different simulation box sizes: (a) 40 x 40 x ∼5 nm^3, (b) 30 x 30 x ∼5 nm^3, (c) 20 x 20 x ∼5 nm^3.

(1)

Table S7: Number of contacts for the different simulation box sizes. The P3HT-P3HT, P3HT-PCBM and PCBM-PCBM contacts are expressed as percentages of the total number of contacts.

simulation box size	P3HT-P3HT (%)	P3HT-PCBM (%)	PCBM-PCBM (%)
20 x 20 x ∼5 nm^3	53.1 ± 0.1	17.6 ± 0.1	29.3 ± 0.1
30 x 30 x ∼5 nm^3	53.5 ± 0.6	17.3 ± 1.1	29.2 ± 0.5
40 x 40 x ∼5 nm^3	53.8 ± 0.4	16.6 ± 0.7	29.6 ± 0.4

Backmapping Details

First, the blend is made *whole*, *i.e.*, molecules which cross the boundaries of the simulation box are not cut but kept whole; this can be done with the GROMACS tool `gmx trjconv`. The volume of the backmapped AA system, as can be deduced from Table S2, is significantly less than its CG version: the lower CG density turns out to facilitate the backmapping step (in terms of numerical stability, *i.e.*, no bad contacts or overlaps). Note that, given the typical large system sizes (∼400000 atoms), the initial minimization step in `initram.sh` may not converge occasionally (too high forces between some of the atoms): restarting the steepest descent, however, solves the problem. As a whole, the backmapping procedure is efficient, taking about 10 minutes on a 12-core machine for typical blends (∼400000 atoms). Subsequent NPT equilibration requires typically less than 10 ns for the density of the backmapped system to converge (typical density evolution shown in Figure S9).

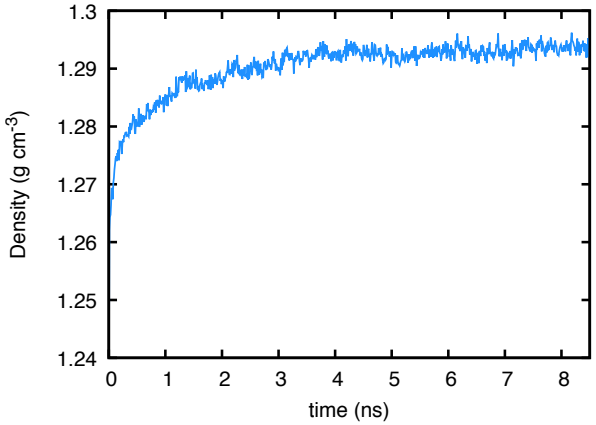

Figure S9: Total blend density evolution of the backmapped blend during relaxation.

Analysis Details

Number of Contacts. Number of contacts are computed employing the `gmx mindist` GROMACS tool with a cutoff distance of 0.6 nm, a length which comprises the nearest neighbour CG sites around a CG particle, the radius of Martini CG particles being $\sqrt[6]{2}\sigma_N = 0.264$ nm (where $\sigma_N = 0.47$ nm). For P3HT-PCBM contacts, the command to be used is:

```
echo 0 1 | gmx mindist -n phases.ndx -f blend.gro -d 0.6 -on P3HT-PCBM.xvg
```

where the GROMACS index `phases.ndx` contains two groups: one to which all the P3HT beads (but the virtual sites) belong and the second to which all the PCBM beads belong; and `blend.gro` contains the coordinates of the molecules in the configuration for which the number of contacts has to be computed. The bash `echo` piped before the `gmx mindist` command will select group 0 (P3HT) and group 1 (PCBM) so to compute the number of contacts between the two groups (i.e., P3HT-PCBM contacts). When computing the pure phases contacts (P3HT-P3HT and PCBM-PCBM) the counting of intramolecular contacts which would follow by employing an index as the one described above is avoided by employing the following procedure. The number of contacts between each P3HT (PCBM) molecule and *all the other* P3HT (PCBM) molecules (therefore practically having to define a separate index file for each molecule considered) are computed separately; this is iterated for all the P3HT (PCBM) molecules and then added together. The sum of all these contacts must then be divided by 2 to remove the double counting arising from computing the contacts between mol_1 and all the other molecules (containing contacts between mol_1-mol_2) and the contacts between mol_2 and all the other molecules (containing contacts between mol_2-mol_1).

Normalization of P3HT-PCBM Contacts. A planar heterojunction and a completely (randomly) intermixed morphologies have been used as the two opposite reference (extreme) cases of mixing to normalize the number of computed P3HT-PCBM contacts. These two configurations have been generated using a starting configuration obtained with the software packmol[S27] which has been then equilibrated in NPT conditions. See Figure

S10. Note that the planar heterojunction configuration contains only one P3HT-PCBM interface.

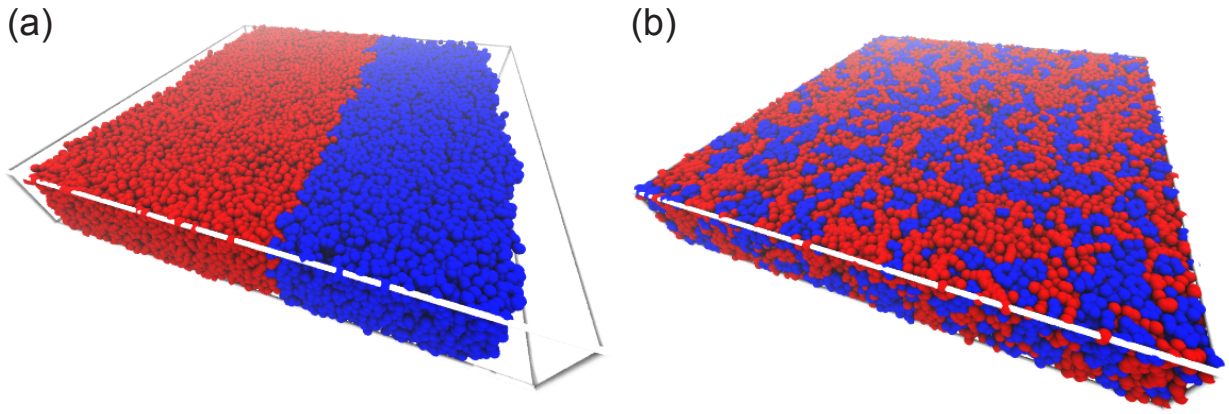

Figure S10: (a) Planar heterojunction and (b) randomly mixed configurations from which, respectively, the minimal and maximal amount of P3HT-PCBM contacts can be extracted.

References

(S1) Masters, R. C.; Pearson, A. J.; Glen, T. S.; Sasam, F.-C.; Li, L.; Dapor, M.; Donald, A. M.; Lidzey, D. G.; Rodenburg, C. *Nat. Comm.* **2015**, *6*, 6928.

(S2) Janeliunas, D. *Self-Assembly of Facial Oligothiophene Amphiphiles*; Ph.D. Dissertation, TU Delft, Delft University of Technology, 2014.

(S3) Bulacu, M.; Goga, N.; Zhao, W.; Rossi, G.; Monticelli, L.; Periole, X.; Tieleman, D. P.; Marrink, S. J. *J. Chem. Theory Comput.* **2013**, *9*, 3282–3292.

(S4) Monticelli, L. *J. Chem. Theory Comput.* **2012**, *8*, 1370–1378.

(S5) `http://perso.ibcp.fr/luca.monticelli/MARTINI/index.html`.

(S6) Bulle-Lieuwma, C. W. T.; van Gennip, W. J. H.; van Duren, J. K. J.; Jonkheijm, P.; Janssen, R. A. J.; Niemantsverdriet, J. W. *App. Surf. Sci.* **2003**, *203*, 547–550.

(S7) Geens, W.; Martens, T.; Poortmans, J.; Aernouts, T.; Manca, J.; Lutsen, L.; Heremans, P.; Borghs, S.; Mertens, R.; Vanderzande, D. *Thin Solid Films* **2004**, *451*, 498–502.

(S8) van Bavel, S.; Sourty, E.; de With, G.; Frolic, K.; Loos, J. *Macromolecules* **2009**, *42*, 7396–7403.

(S9) Kiel, J. W.; Kirby, B. J.; Majkrzak, C. F.; Maranville, B. B.; Mackay, M. E. *Soft Matter* **2010**, *6*, 641–646.

(S10) Dang, M. T.; Hirsch, L.; Wantz, G. *Adv. Mater.* **2011**, *23*, 3597–3602.

(S11) Oostenbrink, C.; Villa, A.; Mark, A. E.; van Gunsteren, W. F. *J. Comput. Chem.* **2004**, *25*, 1656–1676.

(S12) Malde, A. K.; Zuo, L.; Breeze, M.; Stroet, M.; Poger, D.; Nair, P. C.; Oostenbrink, C.; Mark, A. E. *J. Chem. Theory Comput.* **2011**, *7*, 4026–4037.

(S13) Thole, B. T.; van Duijnen, P. T. *Theor. Chim. Acta* **1983**, *63*, 209–221.

(S14) Guest, M. F.; Bush, I. J.; van Dam, H. J. J.; Sherwood, P.; Thomas, J. M. H.; van Lenthe, J. H.; Havenith, R. W. A.; Kendrick, J. *Mol. Phys.* **2005**, *103*, 719–747.

(S15) Darling, S. B.; Sternberg, M. *J. Phys. Chem. B* **2009**, *113*, 6215–6218.

(S16) Girifalco, L. A. *J. Phys. Chem.* **1992**, *96*, 858–861.

(S17) Jorgensen, W. L.; Maxwell, D. S.; Tirado-Rives, J. *J. Am. Chem. Soc.* **1996**, *118*, 11225–11236.

(S18) Cheung, D. L.; Troisi, A. *J. Phys. Chem. C* **2010**, *114*, 20479–20488.

(S19) Lide, D. R. *CRC Handbook of Chemistry and Physics*; CRC press, 2004.

(S20) Bussi, G.; Donadio, D.; Parrinello, M. *J. Chem. Phys.* **2007**, *126*, 014101.

(S21) Parrinello, M.; Rahman, A. *J. App. Phys.* **1981**, *52*, 7182–7190.

(S22) Shirts, M. R.; Chodera, J. D. *J. Chem. Phys.* **2008**, *129*, 124105.

(S23) Abraham, M. H.; Chadha, H. S.; Whiting, G. S.; Mitchell, R. C. *J. Pharm. Sci.* **1994**, *83*, 1085–1100.

(S24) Klamt, A.; Jonas, V.; Bürger, T.; Lohrenz, J. C. W. *J. Phys. Chem. A* **1998**, *102*, 5074–5085.

(S25) Berendsen, H. J. C.; Postma, J. P. M. v.; van Gunsteren, W. F.; DiNola, A.; Haak, J. R. *J. Chem. Phys.* **1984**, *81*, 3684–3690.

(S26) Kumar, S.; Rosenberg, J. M.; Bouzida, D.; Swendsen, R. H.; Kollman, P. A. *J. Comput. Chem.* **1992**, *13*, 1011–1021.

(S27) Martínez, L.; Andrade, R.; Birgin, E. G.; Martínez, J. M. *J. Comput. Chem.* **2009**, *30*, 2157–2164.